Communication

Superconductivity in Metal-Rich Chalcogenide Ta$_2$Se

Xin Gui, Karolina Górnicka, Qiang Chen, Haidong Zhou, Tomasz Klimczuk, and Weiwei Xie*

Cite This: *Inorg. Chem.* 2020, 59, 5798−5802

Read Online

ACCESS | Metrics & More | Article Recommendations | Supporting Information

ABSTRACT: The metal−metal bond in metal-rich chalcogenide is known to exhibit various structures and interesting physical properties. Ta$_2$Se can be obtained by both arc-melting and solid-state pellet methods. Ta$_2$Se crystallizes a layered tetragonal structure with space group $P4/nmm$ (No. 129; Pearson symbol $tP6$). Each unit cell consists of four layers of body-centered close-packing Ta atoms sandwiched between two square nets of Se atoms, forming the Se−Ta−Ta−Ta−Ta−Se networks. Herein, we present magnetic susceptibility, resistivity, and heat capacity measurements on Ta$_2$Se, which together indicate bulk superconductivity with T_c = 3.8(1) K. According to first-principles calculations, the d orbitals in Ta atoms dominate the Fermi level in Ta$_2$Se. The flat bands at the Γ point in the Brillouin zone yield the van Hove singularities in the density of states around the Fermi level, which is intensified by introducing a spin−orbit coupling effect, and thus could be critical for the superconductivity in Ta$_2$Se. The physical properties, especially superconductivity, are completely different from those of Ta-rich alloys or transition-metal dichalcogenide TaSe$_2$.

Transition-metal-rich chalcogenides are a fascinating series of solid-state structures in which several-atom-thick slabs of transition-metal atoms are terminated with monolayers of chalcogenides. Moreover, transition-metal-rich chalcogenides usually share a common structural feature in that the transition metal forms an octahedron or trigonal prism with chalcogen elements in the center,[1−4] which can be considered to be the antiformat of transition-metal dichalcogenides (TM$_2$).[5] The layered transition-metal dichalcogenides have received interest for decades because of their variety in electronic properties in both bulk and surface states.[6−12] However, a limited number of studies of transition-metal-rich chalcogenides, mainly with an emphasis on the structures, have been reported.[13−15] Most metal-rich chalcogenides occur in the earliest transition metals (Sc, Y, and Ti) and especially the late lanthanides.[14−19] Harbrecht discovered the first of these transition-metal-rich chalcogenides, Ta$_2$Se, by a simple arc-melting preparation.[2] Ta$_2$Se can be considered to be an insertion of Se into bulk body-centered close-packing Ta metal, with every four layers of Ta intercalated by two layers of Se. However, isoelectronic Nb$_2$Se has a very different structure, which could be described as built up from condensed octahedral clusters. Considering the extensive metal−metal bonding in these examples, we focused on Ta$_2$Se, which may induce interesting exotic physical properties, for example, superconductivity. Moreover, by comparing the crystal structures of Ta$_2$Se and the well-known 2H-TaSe$_2$, one can easily obtain some significant differences. The layered stacking pattern of 2H-TaSe$_2$ can be seen as (TaSe)SeSe(TaSe), while it is (TaSe)TaTa(TaSe) for Ta$_2$Se. The Ta atoms in TaSe$_2$ are three-coordinated but four-coordinated in Ta$_2$Se. Interestingly, when Cu atoms were intercalated into the TaSe$_2$ van der Waals gap, the superconducting transition temperature can be increased from 0.14 K for pure 2H-TaSe$_2$ to $T_{c,max}$ = 2.7 K Cu$_x$TaSe$_2$.[20] Thus, for Ta$_2$Se, will the intercalation of Ta atoms induce the superconductivity and yield a high T_c?

The preparation of Ta$_2$Se and the phase determination method are shown in the Supporting Information. An obtained Ta$_2$Se chunk from arc melting was determined to contain a small amount of 1T-TaSe$_2$ (P$\bar{3}$m1) as the impurity (∼6.5 wt %). The powder X-ray diffraction (XRD) pattern shown in Figure 1b matches the previously reported Ta$_2$Se pattern very well.[2] To determine if a charge-density wave exists in Ta$_2$Se at low temperatures, similar to the case in TaSe$_2$, we performed low-temperature powder XRD measurements at 100 and 200 K. No superlattice peaks were observed above 100 K for the Ta$_2$Se phase, as shown in Figure S1. This indicates no evidence for the existence of a charge-density wave above 100 K in Ta$_2$Se. As shown in Figure 1a, two crystallographically different Ta sites, marked as Ta1 and Ta2, and one Se site exist in the Ta$_2$Se binary compound. Specifically, the Ta1 bilayer was sandwiched by two edge-shared Ta2@Se$_4$ layers, and the resulting Se−Ta2−Ta1−Ta1−Ta2−Se layers stack along the c axis to form a layered Ta$_2$Se structure. The Ta1−Ta1 and Ta1−Ta2 bonds are 2.831(2) and 2.895(2) Å, respectively, while the Ta2 atoms are separate with Se with a length of 2.665(3) Å. The long Se−Se distance (∼3.57 Å) indicates that van der Waals force bonds the Se−Ta$_4$−Se layers in Ta$_2$Se. Moreover, the chemical composition was also determined by scanning electron microscopy−energy-dispersive X-ray spectroscopy (SEM−EDS), as shown in Table S1 and Figure S2, which indicates a formula of Ta$_{1.92(6)}$Se, and excess Se shows that TaSe$_2$ can be a plausible impurity.

Detailed physical property measurements are described in the Supporting Information. The plot of the volume magnetic susceptibility (χ_V) versus temperature after diamagnetic
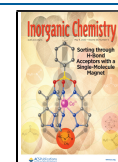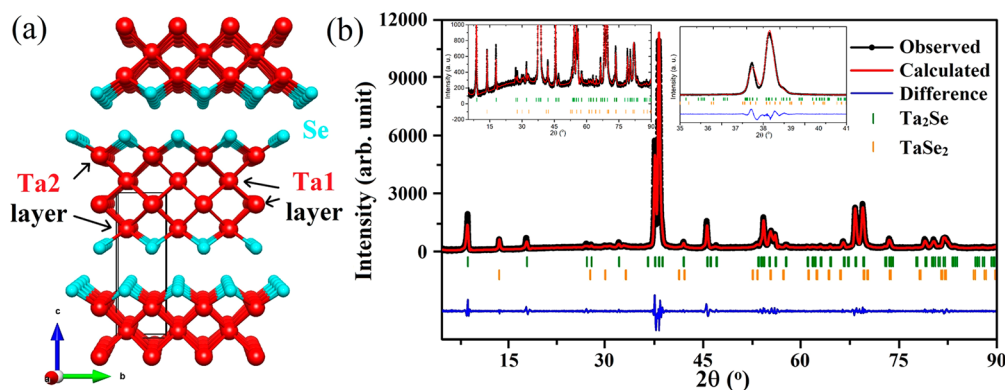
Figure 1. (a) Crystal structure of Ta_2Se, where red and cyan balls represent Ta and Se atoms, respectively. (b) Refined powder XRD pattern for Ta_2Se. The black line with balls, red line, blue line, green vertical ticks, and orange vertical ticks stand for observed and calculated patterns, difference between the observed and calculated patterns, and Ta_2Se and 1T-$TaSe_2$ Bragg peaks. Insets show the magnified versions of powder XRD pattern fitting.
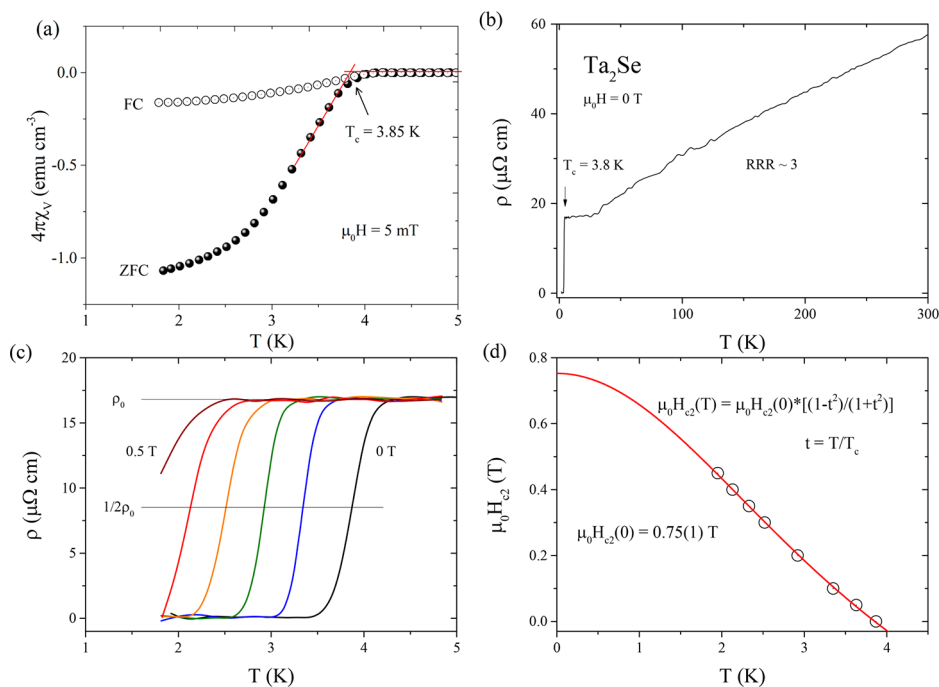

Figure 2. (a) Temperature dependence of the ZFC and FC volume magnetic susceptibilities for Ta_2Se. The data were collected between 1.8 and 5 K in applied magnetic field $\mu_0 H = 5$ mT. (b) Electrical resistivity $\rho(T)$ of Ta_2Se measured in zero magnetic field. (c) Expanded plot of the low-temperature $\rho(T)$ showing the superconducting transition for different magnetic fields from 0 to 0.5 T. Horizontal lines represent a residual resistivity and half of the transition, respectively. (d) Upper critical field $\mu_0 H_{c2}$ versus temperature of Ta_2Se determined from the electrical resistivity $\rho(T,H)$ data in panel c. The red curve is a fit obtained using the G–L equation.

correction is shown in Figure 2a. The large diamagnetic signal below 3.8 K indicates the occurrence of superconductivity in this compound. On the basis of the zero-field-cooled (ZFC) signal, the transition is broad, likely because of the relatively large applied field (50 Oe), and does not saturate even at the lowest available temperature. However, $4\pi\chi_V(2 \text{ K}) = -1.07$, the absolute value of which is larger than that expected for the full Meissner fraction $(4\pi\chi_V = -1)$. This discrepancy is caused by a demagnetization effect and is dependent on the sample shape and its orientation with respect to the direction of the external magnetic field. The field-cooled (FC) signal is much weaker compared to the ZFC signal, usually resulting from strong flux trapping in Ta_2Se and is typically observed in polycrystalline samples. The critical superconducting temperature (T_c) was estimated as the intersection between two lines marked in red in Figure 2a: the first one is the steepest slope line of the

superconducting signal, and the second one is an extrapolation of the normal metal state χ_V to lower temperature.[21] The value thus obtained is $T_c = 3.85$ K, higher than the critical temperature for $TaSe_2$ $(T_c = 0.22 \text{ K}[22])$ and lower than that reported for pure Ta metal $(T_c = 4.4 \text{ K}).[23]$ The width of the transition and the critical temperature decrease with increasing applied magnetic field, and the signal completely vanishes above 3500 Oe. The field dependence of magnetization is shown in Figure S3, which indicates a typical character of type II superconductors.

Subsequently, the resistivity measurements were carried out in the Physical Property Measurement System Quantum Design Dynacool with a four-probe technique. Figure 2b presents the resistivity as a function of the temperature in the range of 1.8– 300 K without application of an external magnetic field. The resistivity undergoes a sudden drop at 3.8 K, which is an indication of superconductivity. In the normal state, the $\rho(T)$

curve exhibits metallic behavior of the Bloch−Grüneisen type. Typical behaviors in the resistivity for polycrystalline metals were observed with a low residual resistivity ratio [RRR = $\rho(300\ \text{K})/\rho(4\ \text{K})$ = 3]. Figure 2c emphasizes the low-temperature resistivity under various magnetic fields from 0 to 0.5 T. At $\mu_0 H$ = 0 T, an abrupt resistivity drop due to the superconducting transition is clearly observed at T_c = 3.8 K. As can be seen, the superconducting transition temperatures were suppressed with larger fields. Above 1.8 K, the zero-resistance behavior is not observed for $\mu_0 H$ = 0.5 T and the resistivity drop disappears for $\mu_0 H$ > 0.75 T (not shown here). Using the criterion that the point with 50% normal state resistivity suppressed can be considered to be the transition temperature, we determined the upper critical field $\mu_0 H_{c2}(T)$ for Ta$_2$Se at various temperatures below 3.8 K (Figure 2d). The data are fitted with the following Ginzburg−Landau (G−L) relationship:[24]

$$\mu_0 H_{c2}(T) = \mu_0 H_{c2}(0)\ \frac{1 - t^2}{1 + t^2}$$

where $t = T/T_c$, in which T_c is a fitting parameter (transition temperature at zero magnetic field). The G−L relation well describes the experimental data, and it yields $\mu_0 H_{c2}(0)$ = 0.75(1) T and T_c = 3.86(1) K. The obtained upper critical field does not exceed the Pauli limiting field for the weak-coupling Bardeen−Cooper−Schrieffer (BCS) superconductors[25] $H_{c2}^P(0)$ = 1.85T_c, which for T_c = 3.8 K gives $H_{c2}^P(0)$ = 7 T. The critical field that we obtained for Ta$_2$Se is over 9 times larger than that reported for elemental Ta ($\sim$0.083 T).[26,27] Even though the critical temperature of Ta$_2$Se decreases from 4.5 to 3.7 K with the insertion of Se layers into Ta layers, the segregation of Ta atoms increases the ability for Ta$_2$Se to resist a magnetic field, which indicates a stronger electron−phonon coupling.

Heat capacity measurement by measuring the entropy changes during the superconducting transition is reliable evidence of the presence of bulk superconductivity. To prove that the superconductivity is intrinsic to Ta$_2$Se and is not a consequence of the possible impurity phases in the sample, such as TaSe$_2$ or Ta, specific heat measurements were conducted on the Ta$_2$Se sample. Superconductivity can be considered to be a "phase" transition, with a superconducting phase transition occurring below the critical temperature. Figure 3a depicts a closer view of the data under zero magnetic field. Bulk superconductivity was also proven by a significant anomaly at 3.8 K, close to the T_c value obtained from resistivity and magnetic measurements. C_p jumps at T_c, estimated by using the equal entropy construction (blue solid lines), are about $\Delta C/T_c$ = 16 mJ mol^{-1} K^{-2}. Figure 3b illustrates the heat capacity behavior of Ta$_2$Se under an external magnetic field of 1 T. The data can be fitted by $C_p/T = \gamma + \beta T^2$, where γ and β are determined by electronic and phononic contributions, respectively. The extrapolation gives γ = 12.4(1) mJ mol^{-1} K^{-2} and β = 0.29(1) mJ mol^{-1} K^{-4}. Furthermore, the Debye temperature can be estimated through the relationship $\Theta_D = \left(\frac{12\pi^4}{5\beta}nR\right)^{1/3}$, where R = 8.314 J mol^{-1} K^{-1} and n = 3 for Ta$_2$Se. The obtained Debye temperature is 271(1) K, which is larger than the value for a pure Ta element (Θ_D = 240 K). Using the Sommerfeld coefficient [γ = 12.4(1) mJ mol^{-1} K^{-2}] and the previously derived specific heat jump at T_c, the superconducting parameter $\Delta C/\gamma T_c$ = 1.29 can be calculated. The obtained value is slightly lower than the theoretical value based on the BCS theory ($\Delta C/\gamma T_c \sim 1.43$),
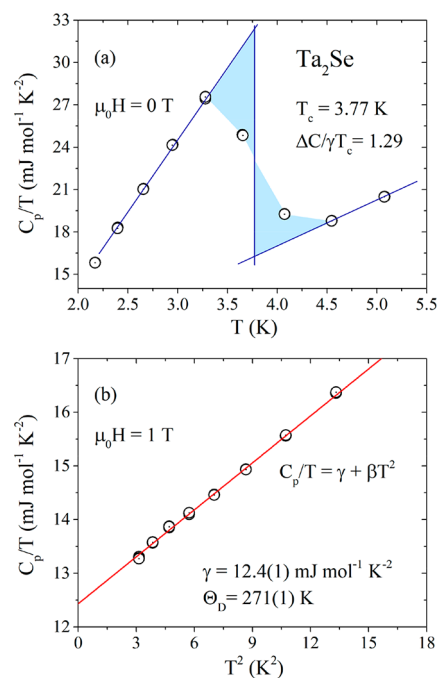

Figure 3. (a) Specific heat anomaly in a zero magnetic field at low temperatures with T_c = 3.77 K. (b) C_p/T versus T^2 plot under a $\mu_0 H$ = 1 T magnetic field.

likely caused by the presence of impurity phases, which is consistent with the powder XRD refinement.

With the Debye temperature available, the electron−phonon constant λ_{e-p} can be obtained through the inverted McMillan equation:[28]

$$\lambda_{e-p} = \frac{1.04 + \mu^* \ln(\Theta_D/1.45T_c)}{(1 - 0.62\mu^*)\ln(\Theta_D/1.45T_c) - 1.04}$$

where μ^* is the repulsive screened Coulomb part. The value of μ^* is usually set to 0.13 for intermetallic superconductors. Using Θ_D = 271(1) K and T_c = 3.8 K (obtained from the specific heat measurements), one obtains λ_{e-p} = 0.61, which suggests weak electron−phonon coupling behavior.

The total band structure and projection (as shown by the band thickness) of the d orbitals in Ta atoms and the p orbitals in Se atoms without including the spin−orbit coupling (SOC) effect are calculated, as illustrated in Figure 4. The Fermi levels are dominated by d electrons from both Ta sites both with and without SOC cases, which indicates the critical role of the metal−metal bond in the stability and superconductivity in Ta$_2$Se. The electrons on the p orbitals from Se atoms mainly contribute $\sim$2.5 eV below the Fermi level to stabilize the structure. The flat bands from the Γ to Z points near the Fermi level, which were mentioned above, are dominated by the d orbitals of Ta atoms and thus lead to a van Hove singularity near the Fermi level in the density of states (DOS). Moreover, after including the SOC effect on Ta atoms, a small band gap ($\sim$100 meV) at the Γ point $\sim$0.1 eV above the Fermi level can be observed. The DOS at the Fermi level was strengthened by $\sim$10% the SOC effects marked in the red arrows were included, which ends up forming a sharp peak at E$_F$. Such an intensive DOS at E$_F$ can result in some electronic instability and exotic physical properties such as superconductivity. Thus, it is highly possible that more metal-rich chalcogenides can host super-conductivity because of the dominant metal−metal interaction.
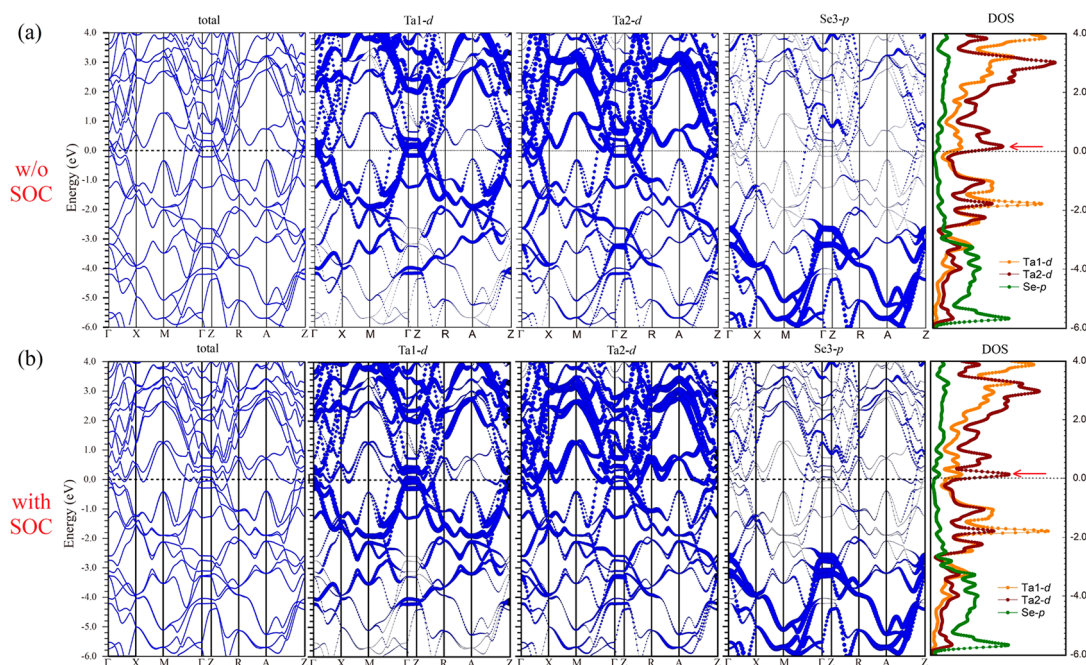
Figure 4. Band structure of Ta_2Se projected from the d orbitals of Ta atoms and the p orbitals of Se atoms, where the thicker the band, the higher the contribution of the corresponding orbital to the band (left three) and DOS of Ta_2Se (right): (a) without consideration of the SOC effect; (b) with consideration of the SOC effect.

In comparison with the DOS of elemental Ta, as shown in Figure S4, one can find that the d character from Ta is dominant around the Fermi level, similar to Ta_2Se. Moreover, a van Hove singularity originating from d electrons can be found ~100 meV above E_F. Note that, in Ta_2Se, the d character from the Ta2 atom shows a similar DOS peak above E_F. This implies the significance of Ta d electrons in superconductivity in the Ta-rich system.

In summary, we report the first metal-rich chalcogenide superconductor Ta_2Se with extensive metal−metal interactions. Ta_2Se was synthesized by the arc-melting method and structurally characterized by powder XRD; the physical properties were measured by magnetism, resistance, and specific heat, and Ta_2Se was discovered to be a new weak-coupling BCS superconductor at $T_c \sim 3.8$ K. The electronic structures analyzed by the *WIEN2k* program indicate the importance of d electrons of Ta atoms in superconductivity and lead to a high probability to discover more superconductors in metal-rich chalcogenides.

■ ASSOCIATED CONTENT

ⓈⒾ Supporting Information

The Supporting Information is available free of charge at https://pubs.acs.org/doi/10.1021/acs.inorgchem.9b03656.

Experimental details, low-temperature powder XRD for Ta_2Se, SEM−EDS results, field dependence of magnetization, and DOS of elemental Ta (PDF)

■ AUTHOR INFORMATION

Corresponding Author

Weiwei Xie − *Department of Chemistry, Louisiana State University (LSU), Baton Rouge, Louisiana 70803, United States;* ⓘ orcid.org/0000-0002-5500-8195; Phone: 225-578-1074; Email: weiweix@lsu.edu

Authors

Xin Gui − *Department of Chemistry, Louisiana State University (LSU), Baton Rouge, Louisiana 70803, United States*

Karolina Górnicka − *Faculty of Applied Physics and Mathematics, Gdansk University of Technology (GUT), Gdansk 80-233, Poland*

Qiang Chen − *Department of Physics, University of Tennessee, Knoxville, Tennessee 37996, United States*

Haidong Zhou − *Department of Physics, University of Tennessee, Knoxville, Tennessee 37996, United States*

Tomasz Klimczuk − *Faculty of Applied Physics and Mathematics, Gdansk University of Technology (GUT), Gdansk 80-233, Poland;* ⓘ orcid.org/0000-0002-7089-4631

Complete contact information is available at:
https://pubs.acs.org/10.1021/acs.inorgchem.9b03656

Notes

The authors declare no competing financial interest.

■ REFERENCES

(1) Maggard, P. A.; Corbett, J. D. Sc_2Te: A Novel Example of Condensed Metal Polyhedra in a Metal-Rich but Relatively Electron-Poor Compound. *Angew. Chem., Int. Ed. Engl.* **1997**, *36*, 1974−1976.

(2) Harbrecht, B. Ta_2Se: A Tantalum-Rich Selenide with a New Layer Structure. *Angew. Chem., Int. Ed. Engl.* **1989**, *28*, 1660−1662.

(3) Kim, S. J.; Nanjundaswamy, K. S.; Hughbanks, T. Single-Crystal Structure of Tantalum Sulfide (Ta_3S_2). Structure and Bonding in the Ta_6Sn (n = 1,3,4,5?) Pentagonal-Antiprismatic Chain Compounds. *Inorg. Chem.* **1991**, *30*, 159−164.

(4) Abdon, R. L.; Hughbanks, T. Hf$_3$Te$_2$: Ein Neues Tellurid Mit Bemerkenswerter Schichtstruktur. *Angew. Chem.* **1994**, *106*, 2414−2416.

(5) Giester, G.; Lengauer, C. L.; Tillmanns, E.; Zemann, J. Tl$_2$S: Re-Determination of Crystal Structure and Stereochemical Discussion. *J. Solid State Chem.* **2002**, *168*, 322−330.

(6) Mattheiss, L. F. Band Structures of Transition-Metal-Dichalcogenide Layer Compounds. *Phys. Rev. B* **1973**, *8*, 3719−3740.

(7) Zhu, Z. Y.; Cheng, Y. C.; Schwingenschlögl, U. Giant Spin-Orbit-Induced Spin Splitting in Two-Dimensional Transition-Metal Dichalcogenide Semiconductors. *Phys. Rev. B: Condens. Matter Mater. Phys.* **2011**, *84*, 153402.

(8) Ayari, A.; Cobas, E.; Ogundadegbe, O.; Fuhrer, M. S. Realization and electrical characterization of ultrathin crystals of layered transition-metal dichalcogenides. *J. Appl. Phys.* **2007**, *101*, 014507.

(9) Dawson, W. G.; Bullett, D. W. Electronic Structure and Crystallography of MoTe$_2$ and WTe$_2$. *J. Phys. C: Solid State Phys.* **1987**, *20*, 6159−6174.

(10) Coehoorn, R.; Haas, C.; Dijkstra, J.; Flipse, C. J. F.; de Groot, R. A.; Wold, A. Electronic structure of MoSe$_2$, MoS$_2$, and WSe$_2$. I. Band-structure calculations and photoelectron spectroscopy. *Phys. Rev. B: Condens. Matter Mater. Phys.* **1987**, *35*, 6195−6202.

(11) Luo, H.; Xie, W.; Tao, J.; Inoue, H.; Gyenis, A.; Krizan, J. W.; Yazdani, A.; Zhu, Y.; Cava, R. J. Polytypism, Polymorphism, and Superconductivity in TaSe$_{2-x}$Te$_x$. *Proc. Natl. Acad. Sci. U. S. A.* **2015**, *112* (11), E1174−E1180.

(12) Liu, Y.; Shao, D. F.; Li, L. J.; Lu, W. J.; Zhu, X. D.; Tong, P.; Xiao, R. C.; Ling, L. S.; Xi, C. Y.; Pi, L.; et al. Nature of Charge Density Waves and Superconductivity in 1T-TaSe$_{2-x}$Te$_x$. *Phys. Rev. B: Condens. Matter Mater. Phys.* **2016**, *94*, 045131.

(13) Chen, L.; Corbett, J. D. Remarkable Metal-Rich Ternary Chalcogenides Sc$_{14}$M$_3$Te$_8$ (M = Ru, Os). *J. Am. Chem. Soc.* **2003**, *125*, 1170−1171.

(14) Herle, P. S.; Corbett, J. D. The First Metal-Rich Binary Chalcogenides of the Lanthanides: Dy$_2$Te and Gd$_2$Te. *Inorg. Chem.* **2001**, *40*, 1858−1864.

(15) Maggard, P. A.; Corbett, J. D. Sc$_5$Ni$_2$Te$_2$: Synthesis, Structure, and Bonding of a Metal-Metal-Bonded Chain Phase, a Relative of Gd$_3$MnI$_3$. *Inorg. Chem.* **1999**, *38*, 1945−1950.

(16) Weirich, T. E.; Pottgen, R.; Simon, A. Crystal Structure of Octatitanium Triselenide, Ti$_8$Se$_3$. *Z. Kristallogr. - Cryst. Mater.* **1996**, *211*, 929−930.

(17) Castro-Castro, L. M.; Chen, L.; Corbett, J. D. Condensed Rare-Earth Metal-Rich Tellurides. Extension of Layered Sc$_6$PdTe$_2$-Type Compounds to Yttrium and Lutetium Analogues and to Y$_7$Te$_2$, the Limiting Binary Member. *J. Solid State Chem.* **2007**, *180*, 3172−3179.

(18) Maggard, P. A.; Corbett, J. D. Sc$_9$Te$_2$: A Two-Dimensional Distortion Wave in the Scandium-Richest Telluride. *J. Am. Chem. Soc.* **2000**, *122*, 838−843.

(19) Maggard, P. A.; Corbett, J. D. The Synthesis, Structure, and Bonding of Sc$_8$Te$_3$ and Y$_8$Te$_3$. Cooperative Matrix and Bonding Effects in the Solid State. *Inorg. Chem.* **1998**, *37*, 814−820.

(20) Li, X. C.; Zhou, M. H.; Yang, L. H.; Dong, C. Significant enhancement of superconductivity in copper-doped 2H-TaSe$_2$. *Supercond. Sci. Technol.* **2017**, *30*, 125001.

(21) Klimczuk, T.; Cava, R. J. Carbon isotope effect in superconducting MgCNi$_3$. *Phys. Rev. B: Condens. Matter Mater. Phys.* **2004**, *70*, 212514.

(22) Van Maaren, M. H.; Schaeffer, G. M. Some new superconducting group Va dichalcogenides. *Phys. Lett. A* **1967**, *24*, 645−646.

(23) Worley, R. D.; Zemansky, M. W.; Boorse, H. A. Heat capacities of vanadium and tantalum in the normal and superconducting phases. *Phys. Rev.* **1955**, *99*, 447.

(24) Tinkham, M.; Emery, V. Introduction to Superconductivity. *Phys. Today* **1996**, *49*, 74.

(25) Clogston, A. M. Upper limit for the critical field in hard superconductors. *Phys. Rev. Lett.* **1962**, *9*, 266.

(26) Shaw, R. W.; Mapother, D. E.; Hopkins, D. C. Critical fields of superconducting tin, indium, and tantalum. *Phys. Rev.* **1960**, *120*, 88.

(27) Hinrichs, C. H.; Swenson, C. A. Superconducting critical field of tantalum as a function of temperature and pressure. *Phys. Rev.* **1961**, *123*, 1106.

(28) McMillan, W. L. Transition temperature of strong-coupled superconductors. *Phys. Rev.* **1968**, *167*, 331.